Fluorescent Imaging Probe Targeting Mitochondria Based on Supramolecular Host−Guest Assembly and Disassembly

Ning Chu,[⊥] Lili Cong,[⊥] Jing Yue, Weiqing Xu, and Shuping Xu*

ACCESS | Metrics & More | Article Recommendations | SI Supporting Information

ABSTRACT: Fluorescent dyes and probes play an indispensable role in bioimaging. The mitochondrion is one of the crucial organelles which takes charge of energy production and is the primary site of aerobic respiration in the cell. To illuminate mitochondria, a series of supramolecular fluorescent imaging probes were developed based on the host−guest assembly of 1,4-bis[2-(4-pyridyl)ethenyl]-benzene (BPEB) derivatives and cucurbituril[6] (CB[6]). These host−guest conjugates can be efficiently internalized into cells due to their water solubility and target mitochondria according to their positive charges. In response to the intracellular microenvironments, these conjugates start dynamic disassembly. The released BPEBs show a highly hydrophobic feature, which can crystallize to form fluorescent solids that illuminate the mitochondria. The intracellular disassembly of the host−guest probes was evidenced by fluorescence lifetime imaging in situ. These smart mitochondrion-targeting fluorescent imaging probes can be available to investigate the structures and functions of mitochondria, which are of great significance in the intracellular dynamic transformation of supramolecular assemblies.
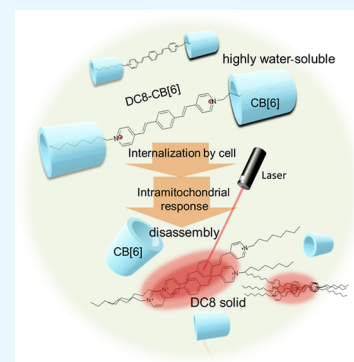
1. INTRODUCTION

Fluorescent dyes and probes play an increasingly important role in the field of biochemistry and bioimaging.[1−5] By proper fluorescent labeling or recognition,[6] real-time fluorescent imaging of specific biomolecules[7,8] and physiological processes[9] can be observed. The continuous innovation and development of cell biology have put forward new requirements for fluorescent probes.[1] Probes with cellular region-targeting features are valuable for studying the functions and morphologies of specific organelles under fluorescent imaging. To achieve organelle-specific imaging, the probes usually feature charges or stimulus-responsive properties to intracellular species, such as reactive oxygen species, metal ions,[10,11] anions,[12,13] biological sulfides,[14,15] specific overexpression proteases[4,13] in cancerous cells, and cell microenvironments, including viscosity, polarity, pH, and so forth.[16,17] Within many developed organelle-specific probes, supramolecular probes have been attractive in recent years due to their flexible stimulus-responsive characteristics.[12,18] The assembly−disassembly processes of these supramolecular conjugates have also been applied for targeting drug delivery and theranostic studies.[19] The mitochondrion is one of the crucial organelles in cells. It plays many vital roles in intracellular physiological processes, including energy conversion, oxidative stress, metabolism, stress responses, cell death, and so forth.[19−21] Mitochondrion-specific fluorescent probes are various,[22,23] and they can be cataloged by mitochondrial membrane potential (JC-1, JC-9, TMRE, Rh123, etc.), mitochondrial mass (e.g., nonyl acridine orange, and MitoTracker series), and mitochondrial reactive oxygen species (MitoSOX and

MitoPY-1).[24−26] In combination with fluorescence imaging, mitochondrial structures and functions can be explored.[8]

1,4-Bis[2-(4-pyridyl)ethenyl]-benzene(BPEB) has a unique symmetric structure and contains multiple double bonds. The [2 + 2] photodimerization reaction can occur between the molecules.[27−30] The pyridine group is a Lewis base, which can coordinate with a variety of metal ions and can also form crystals with hydroxyl groups through hydrogen bonding and with halogen atoms through halogen−nitrogen interaction. BPEB molecules and their derivatives have attracted much attention due to their unique structural characteristics of double bonds and pyridine groups and are widely used in coordination compounds, metal−organic frameworks, cocrystals, molecular assembly, and other fields.[30]

Here, a series of supramolecular host−guest assembly-based fluorescent imaging probes, BPEB derivatives (DC*n*: *n* = 8, 12, and 16), and cucurbituril[6] (CB[6]) conjugates were developed, for mitochondrion-specific imaging.[31] These DC*n*-CB[6] conjugates are positively charged and water-soluble, which assist them in being highly internalized in mitochondria. Due to the dynamic disassembly in response to intracellular microenvironments, these probes dissociate and

release hydrophobic BPEB derivatives, forming fluorescence radiative solids that illuminate mitochondria. The biocompatibility of these supramolecular mitochondrion-specific probes was assessed. These fluorescent imaging probes targeting mitochondria based on supramolecular host—guest assembly and disassembly can be applied to investigate the mitochondrial functions and structures in mitochondrion-related studies. The novelty of this study can be summarized in three aspects, (1) a series of supramolecular host—guest assemblies were achieved, and their disassembly can light up the mitochondria selectively. (2) The disassembly of DC8-CB[6] is the intracellular microenvironment-responsive. (3) The fluorescence imaging of mitochondria was assigned to the crystalline DC8 with a low dissolubility, and a switch of crystallinity of DC8 under the intracellular condition was achieved.

2. EXPERIMENTAL SECTION

2.1. Materials. Terephthalaldehyde (A.R. Aladdin), acetic anhydride (A.R. Beijing Chemical Works), zinc chloride (A.R. Beijing Chemical Works), 4-methylpyridine (A.R. Aladdin), 1-bromine octane (A.R. Aladdin), 1-bromododecane (A.R. Aladdin), 1-bromohexadecane (A.R. Aladdin), glycoluril (A.R. Aladdin), methanal (A.R. Beijing Chemical Works), hydrochloric acid (A.R. Beijing Chemical Works), sulfuric acid (A.R. Beijing Chemical Works), acetone, and ethanol (A.R. Beijing Chemical Works) were obtained.

MCF-7 (human breast cancer cell line), HepG2 (human liver cancer cell carcinoma), and HeLa (human cervical cancer cell line) were bought from the Shanghai ATCC cell bank issued with the permission of the Human Research Ethics Committee of the country for manipulation of human's cells. The WST-1 kit, culture media (DMEM), and fetal bovine serum (FBS) were obtained from JIBCO. Phosphate-buffered-saline solution (PBS, pH = 7.4) was obtained from Beijing Chemical Reagent Company.

2.2. Characterizations. A nuclear magnetic resonance spectrometer 500 MHz (NMR, Avance III 500, Brucker, Switzerland), a nuclear magnetic resonance spectrometer 600 MHz (NMR, Avance III 600, Brucker, Switzerland), a differential scanning calorimeter (DSC204, NETZSCH, Germany), and a high-resolution liquid chromatography—mass spectrometry system (Agilent1290-micrOTOF Q II, Bruker, Switzerland) were used. The solid ultraviolet spectra of DCn and their CB[6] conjugates were collected using a Lambda 950 ultraviolet—visible near-infrared spectrophotometer (PerkinElmer), and the back base was barium sulfate. Fluorescence spectroscopy (RF-5301 pc, Shimadzu) was used to characterize the probes with an excitation light of 473 nm. We measured the quantum yield of DC8 in solid by the time-correlated single-photon counting method via a steady/transient fluorescence spectrometer (Edinburgh Instruments, FLS980) equipped with an integrating sphere. An inverted fluorescence microscope (IX71, Olympus) with an imaging charge-coupled device was employed to take the fluorescent image of DC microcrystals. A ×20, NA = 0.4 lens was employed. Olympus Fluoview Ver.16b software was used to deal with images, and the "colocalization" button was used to plot the scatter graph and calculate Pearson's correlation coefficient.

A Leica STALLARIS 8 scanning confocal microscope equipped with a white laser (450–790 nm) and a 405 nm laser was employed, and FALCON and TauSense functions were used for fluorescent lifetime imaging (FLIM). A ×63 oil lens was used for imaging, and the excitation wavelength was set as 458 nm. The lifetime was analyzed by fitting data from the region of interest (ROI).
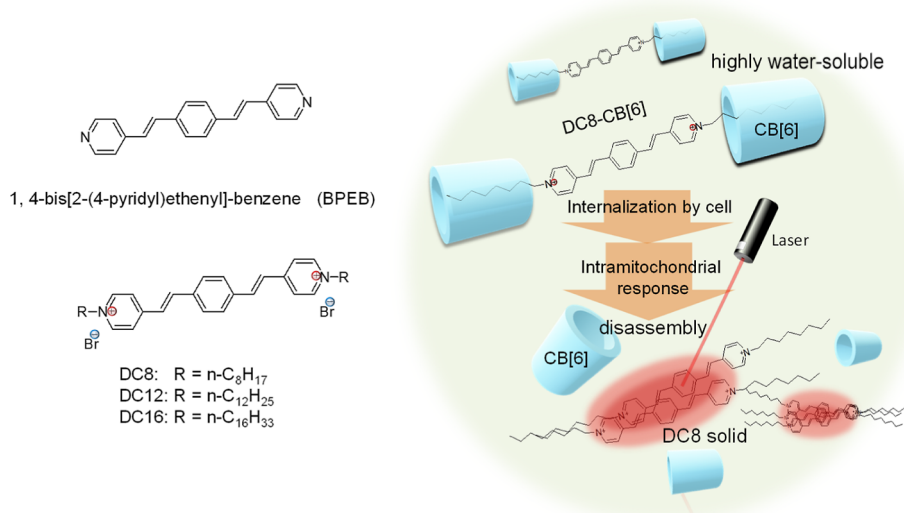
2.3. Synthesis of BPEB Derivatives, CB[6], and Their Assembles. BPEB was first synthesized following the literature.[32] Zinc chloride (13.64 g) was added to a solution containing 13.7 g of 4-methylpyridine and 6.7 g of *p*-phthalaldehyde in 40 mL of acetic anhydride. The mixture was heated for 8 h under reflux, cooled to room temperature, and filtered. The precipitate (yellowish powder) was washed with ethanol and recrystallized from pyridine.

DC8, DC12, and DC16 were synthesized according to the literature.[30] The synthetic method of DC8 was as follows. BPEB (2.86 g) and 1-bromooctane (5.79 g) with a molar ratio of 1:3 were mixed in 200 mL of DMF. The remaining procedures were the same as those for BPEB. DC12 and DC16 were prepared using the same procedures as DC8, except that 1-bromooctane was replaced with 1-bromododecane or 1-bromohexadecane. The molar ratio of BPEB was still kept at 1:3. The coarse products were recrystallized from ethanol. the ^1H NMR, ^{13}C NMR, and MS characterizations of BPEB and DCn (n = 8, 12, and 16) are provided in our previous publication.[33]

Cucurbituril[6] (CB[6]) is synthesized according to the literature.[34] The mixture containing 5.68 g of glycide (40 mmol), 7.0 mL of formaldehyde solution (37% w/w), and 20 mL of sulfuric acid (9.0 M) was heated at 75 °C for 24 h and then heated at 100 °C for another 12 h. After pouring the mixture into 200 mL of deionized water, we added 1.0 L of acetone to produce precipitates thoroughly. The products experienced vacuum extraction, filtration, and cleaning with a water/acetone 1:4 solution. The obtained products were transferred to a 500 mL beaker. 300 mL of water/acetone (1:2, v/v) solution was added, and it was stirred at room temperature for 1 h. CB[6] was obtained by filtration using a vacuum pump. The NMR and MS characterization of CB[6] are provided in the Supporting Information (Figures S1 and S2).

DC8-CB[6] DC8 was dissolved in DMSO at 1.0×10^{-4} mol/L. CB[6] was dissolved in H_2O at 1.0×10^{-5} mol/L. DC8 and CB[6] were mixed and diluted to a specific concentration by H_2O. The molar ratio (DC8/CB[6]) was 1:4. Different molar ratios of DC8 and CB[6] were also optimized, as shown in the Supporting Information (Figure S3).

2.4. Cellular Toxicity Assessment (WST-1 Assay). Before the probes were applied for cellular experiments, the cellular viabilities of MCF-7 cells after they were incubated with different concentrations of supramolecular probes were tested by the WST-1 assay [2-(4-iodophenyl)-3-(4-nitro-phenyl)-5-(2, 4-disulfophenyl)-2H-tetrazolium, monosodium salt]. The MCF-7 cells were grown in the Iscove's modified Dulbecco's medium (IMDM, Gibco) supplemented with 4.5 g/L of glucose and sodium pyruvate, 10% v/v of FBS (Mediatech), and 1% of antimycotic solution (Mediatech). Cell cultures were maintained at 37 °C in a 5% CO_2 humidified incubator. MCF-7 (human breast cancer cell line) were cultured in 96-well plates for 24 h. The cells were cultured with a fresh culture medium containing different concentrations (1.0×10^{-5}, 1.0×10^{-6}, 1.0×10^{-7}, 1.0×10^{-8}, and 1.0×10^{-9} mol/L) of DC8, DC12, DC16, DC8-CB[6], DC12-CB[6], and DC16-CB[6] for 20 min. Then, the probes were removed and washed with PBS. Next, 10 μL of the WST-1 solution in 90 μL of the cell culture medium was added to

Scheme 1. Structures of BPEB, DC8, DC12, and DC16[a]

1, 4-bis[2-(4-pyridyl)ethenyl]-benzene (BPEB)

DC8: R = n-C$_8$H$_{17}$
DC12: R = n-C$_{12}$H$_{25}$
DC16: R = n-C$_{16}$H$_{33}$

[a]Schematic diagrams of the supramolecular host−guest assembly (DC8-CB[6]), its intracellular disassembly, and forming fluorescent DC8 solid in mitochondria.

each well, and the plate was further incubated for 2 h. Finally, the optical density values at 450 nm were recorded by a microplate reader (Tecan Sunrise) to calculate cell viability. The cells without any treatment were used as the control group.

2.5. Colocalization Fluorescence Imaging. Cells were seeded on a clean glass slide to grow to the proper density. They were cultured in the culture plate with 1.0 μM of supramolecular probes for 15 min. After incubation, the coverslips were cleaned three times with PBS, each time for 5 min. Then, cells were incubated with MitoTracker Green for 20 min at room temperature in the dark. After removing the staining dyes by washing with PBS three times, the cells were fixed with 4% formaldehyde for 20 min at room temperature and further cleaned with PBS. The fluorescence images were taken under a laser scanning confocal microscope (Olympus FV1000). Pearson's correlation coefficient was calculated from the whole cell region by the colocalization function of Olympus Fluoview software (ver. 16b), and the graph indicating the colocation quantification was presented and overlap indices were provided as well.

It should be noted that we set 543 nm for our probe in colocalization experiments. The maximum excitation wavelength and emission wavelength of MitoTracker Green are 490 and 516 nm, respectively. The absorption range of MitoTracker Green is from 400 to 530 nm. In order to avoid the crosstalk from MitoTracker Green (λ_{ex} = 488 nm, λ_{em} = 500 nm), λ_{ex} = 543 nm was selected for DC8 solid, while λ_{em} = 610 nm.

2.6. Fluorescence Lifetime Imaging. The MCF-7 cells were seeded and grown in a glass-bottom dish. Our developed probe, DC8-CB[6] with a concentration of 1.0 μM, was added and incubated with cells for 15 min. Then, the cells were washed with a cell culture medium, and they were measured by FALCON and TauSense functions of a Leica STALLARIS 8 laser scanning confocal microscope for FLIM. A ×63 oil lens was used for imaging. λ_{ex} = 458 nm and λ_{em} = 500−600 nm.

3. RESULTS AND DISCUSSION

3.1. Characterization of the Host−Guest Supramolecular Probes. The complex supramolecular probes are composed of a cucurbituril[6] (CB[6]) as a host and BPEB derivatives[35] as a guest. Three BPEB derivatives by grafting BPEB with different lengths of chains were synthesized by following the literature,[30,34,36] denoted DC8, DC12, and DC16 (Scheme 1), respectively. DC8 has an octane structure, and it is a water-carrying molecule. CB[6] has a cavity with an inner diameter of 0.58 nm and a height of 0.91 nm.[37] It can be a host for the host−guest assembly through hydrogen bonding,[38] electrostatic interaction,[39] and other supramolecular interactions.[40,41] Owing to the size limitation, CB[6] can be a nest for the alkyl chain of the guest molecule, and the guest accommodated in its cavity is no more than one molecule.[42−45] Figures S1 and S2 show the ^{1}H NMR and mass spectra of CB[6] we used in this study. The BPEB derivatives can assemble with CB[6] to produce supramolecular structures (Scheme 1), DC8-CB[6], which improves its water solubility and cellular internalization as well. The synthesis procedures of the supramolecular host−guest assemblies are stated in the Supporting Information.[30,34,36] The assembly of DC8 in CB[6] was characterized by NMR and fluorescence spectra. Taking DC8 in CB[6] as an example, we first analyzed the ^{1}H NMR spectra of the achieved DC8-CB[6], as shown in Figure 1. The assignments of ^{1}H NMR spectra of DC8 are shown in Table S1. The chemical shifts (5.5−6.0, 4.0−4.5) belong to CB[6]. The chemical shifts (0.75−1.5) belong to the alkyl chain (H$_a$−H$_f$), while the chemical shifts (8.76, 8.75) are assigned to the pyridine group H$_h$. The chemical shifts (8.21, 8.20) belong to the pyridine group H$_i$. When CB[6] was combined with DC8, the chemical shift of DC8 was kept unchanged (Figure 1A). The peak profiles change at H$_a$−H$_f$ (0.75−1.5), H$_h$ (8.76, 8.75), and H$_i$ (8.21, 8.20) in Figure 1B−D. Owing to the ^{1}H NMR results, CB[6] traps the alkyl chain and pyridine group of DC8, as presented in Scheme 1. To further confirm the location of CB[6] assembled with DC8, a 2D NOESY NMR spectrum of CB[6]-DC8 was recorded (Figure 1F). Region (a)
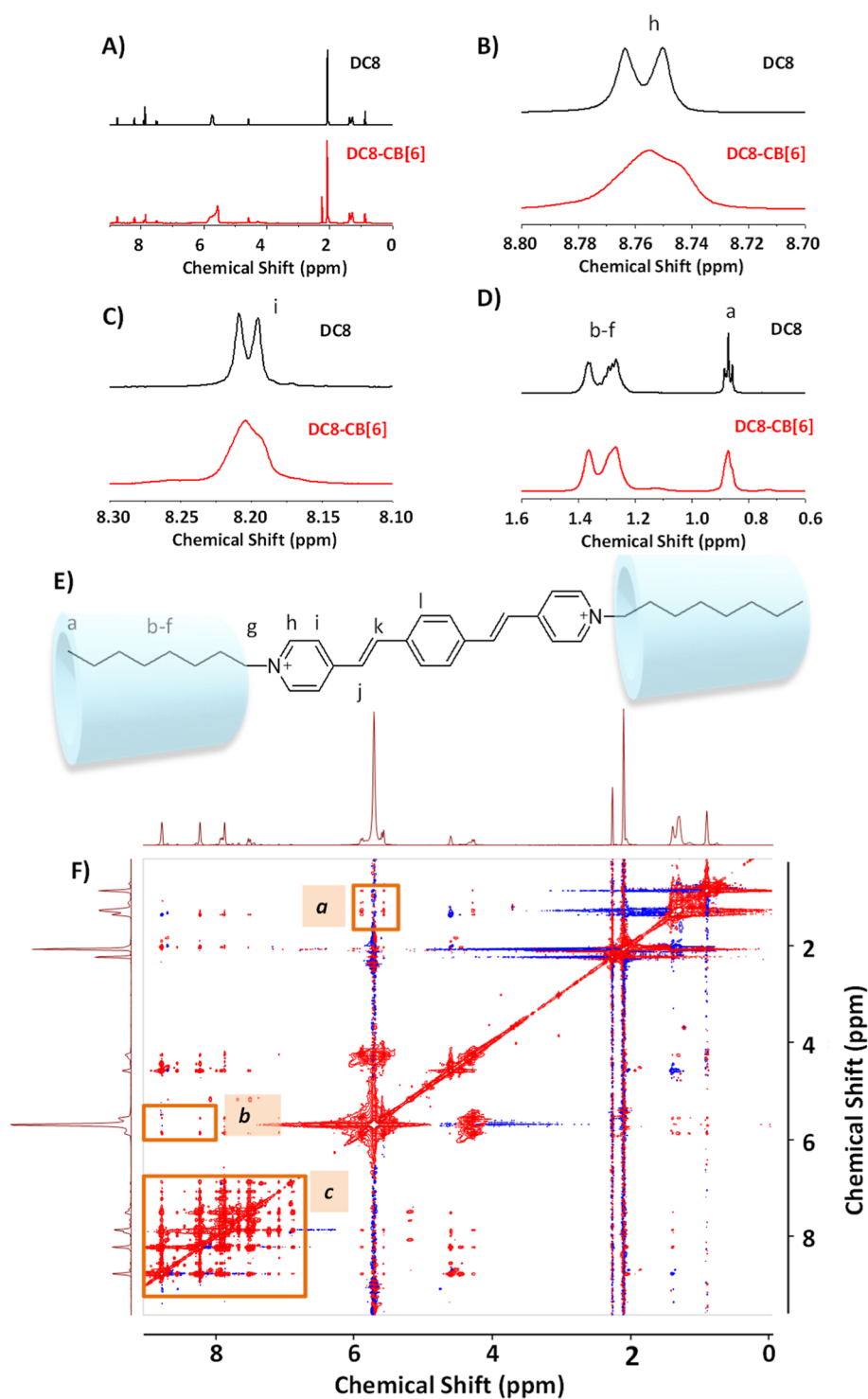
Figure 1. (A) Sections of ^{1}H NMR spectra (500 MHz, acetic acid-d6/D_2O = 1:1) of DC8 and DC8-CB[6]. (B–D) Enlarged ranges of (A). (E) Diagram of DC8-CB[6]. (F) 2D NOESY NMR spectrum (600 MHz, acetic acid-d4/D_2O = 1:1) of CB[6] and DC8.

is the effect between CB[6] and the alkyl chain, while region (b) refers to the effect between CB[6] and the pyridine group. From this, we can prove that CB[6] nests the alkyl chain and pyridine group of DC8, as shown in Figure 1E. Region (c) reflects the effect of the structure of BPEB. We can deduce that the lumen of CB[6] cannot accommodate two benzenes because of its limited size.[35,46] Because the number of dissociative DC8 was large, a ratio of 1:4 of DC8/CB[6] was selected in the present study. When DC8 was mixed with

different concentrations of CB[6], the fluorescence peak at 472 nm remained unchanged (Figure S3), indicating that the binding of DC8 with CB[6] is not located at the chromophore of BPEB.

3.2. Crystallization of DC8 and Its Fluorescence Feature. The crystallization of DC8 and its solid fluorescence were investigated by changing solvents with different ethanol-to-water ratios, in which ethanol and water are the excellent and poor solvents for DC8. With the water ratio increasing, we
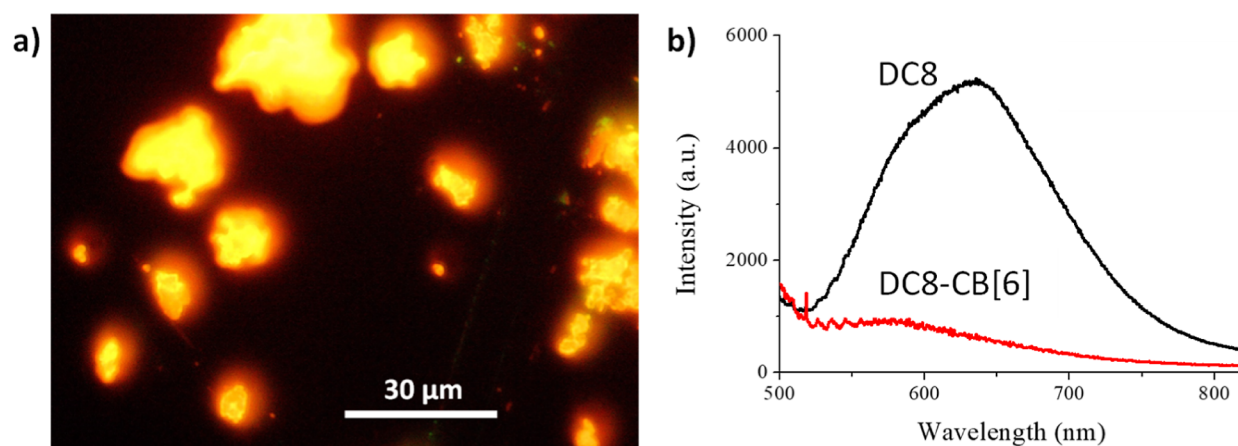
Figure 2. (a) Fluorescence image of the DC8 under the excitation wavelength of 458 nm. (b) Fluorescence spectra of DC8 solid (in ethanol) and DC8-CB[6] (in water) under the excitation wavelength of 473 nm. The concentration is 1.0 μM. The pH value was controlled at 5.3.
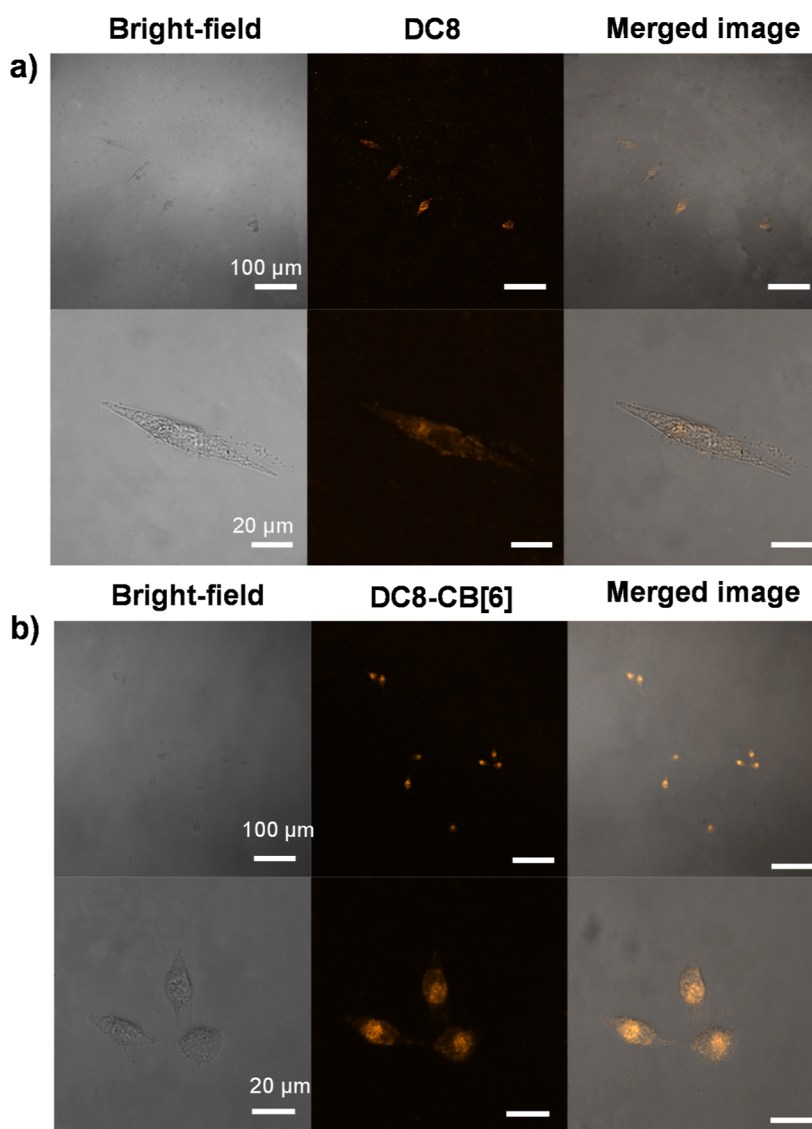

Figure 3. Bright-field (left), fluorescent (middle), and merged (right) images of MCF-7 after they were incubated with DC8 (a) or DC8-CB[6] (b); λ_{ex} = 458 nm, λ_{em} = 600 nm. The concentration of DC8 was 1.0×10^{-6} mol/L. DC8-CB[6] was achieved at a DC8:CB[6] ratio of 1:4.

can observe the microcrystals produced, exhibiting solid-state photoluminescence (PL). Figure 2a displays the fluorescence

image of DC8 in ethanol, showing that solid DC8 emitted bright fluorescence. The fluorescence spectra indicate that the
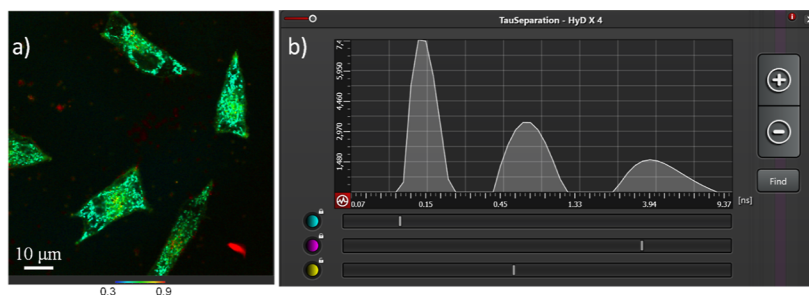
Figure 4. FLIM image (a) of MCF-7 cells incubated with DC8-CB[6]; the image can be fitted as three lifetimes (b) obtained by TauSeparation functions of Leica STELLERIS 8 confocal microscope.
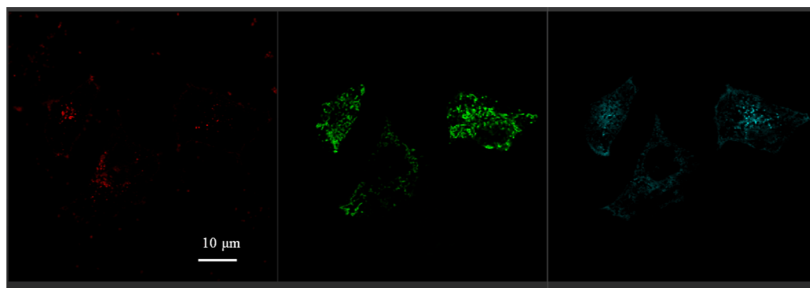
Figure 5. Three lifetime component distributions (red, green, and sapphire) of the DC8-CB[6] incubated MCF-7 cells, obtained by the FALCON function of Leica STELLERIS 8 confocal microscope. Images from left to right correspond to DC8-CB[6], DC8 solid, and DC8 molecules, corresponding to 4.979, 0.348, and 0.851 ns, respectively.

emission band is located at about 635 nm. For DC8-CB[6], they show relatively weak fluorescence in this range under the excitation of 473 nm. If 365 nm light was used for excitation, DC8-CB[6] will emit 472 nm light (Figure S3). We also measured the quantum yield of the DC8 solid as 4.50%.

DC8 is the *N*-alkyl pyridine salt of BPEB. Since alkyl has eight carbons and BPEB is hydrophobic, DC8 has poor water solubility. DC8 can emit green fluorescence under an excitation light of 365 nm in a solution state. However, when the solution environment changes, the aggregation form will appear, and the fluorescence property of the solid state will be displayed. It emits orange−yellow fluorescence at 400−500 nm excitation light. In order to change the solubility of DC8, we assembled it with CB[6]. When the assembly is swallowed into the mitochondria of the cell, DC8 is released because the long alkyl chain in the mitochondria is assembled with CB[6]. Due to its hydrophobic nature, DC8 precipitates and the DC8 solid emits fluorescence at a central wavelength of 600 nm under an excitation light of 400−500 nm, thus achieving fluorescence imaging of mitochondria.

3.3. Biocomparability of the Probes. To apply DC8-CB[6] for cellular experiments, its cellular toxicity was first assessed (Figures S4 and S5). Figure S4 shows the cellular viabilities of MCF-7 cells after they were incubated with different concentrations of DC8(a), DC12(b), DC16(c), DC8-CB[6](d), DC12-CB[6](e), and DC16-CB[6](f) at different concentrations for 15 min, assessed by the WST-1 assay. It can be seen that the cells in 1.0 μM DC8-CB[6] have high viability (Figure S4d). For higher concentrations above 1.0 μM, more dead cells will be obtained. We also assessed the cellular viabilities of MCF-7 cells for individual DC8. As shown in Figure S4a, the acceptable concentration of DC8 for MCF-7 cells was 1.0 μM. We also assessed the cell survival rates of MCF-7 (human breast cancer cell line) and HEK-293T (human embryonic kidney cell line) cells incubated with DC8-

CB[6] at different concentrations for 24 h (Figure S5). It can be observed that 1.0 μM DC8-CB[6] shows low toxicity for cancer and normal cells. Thus, we chose the DC8-CB[6] concentration of 1.0 μM for further cell imaging experiments. This concentration (1.0 μM) is also a safe dosage for DC12, DC16, DC12-CB[6], and DC16-CB[6] (Figure S4).

3.4. Bioimaging of Mitochondria by the Supramolecular Probes. The fluorescent images of MCF-7 cells incubated with DC8-CB[6] (1.0 μM) and individual DC8 (1.0 μM) were obtained and compared. It can be observed in Figure 3a that the hydrophobic DC8 tends to form precipitates in water solutions, which is not conducive to cell internalization and gives a weak imaging contrast. In the case of using DC8-CB[6], its water solubility has been improved (Figure 3b). After internalizing them in cells, the phospholipid in mitochondria causes them to disassemble. Phospholipids contain alkyl chains of different lengths, with different binding constants with CB[6].[47] The length of the alkyl chain does not depend linearly on binding constants. Hence, we guess that the phospholipid may lead DC8-CB[6] to disassembly by replacing the DC8 from DC8-CB[6]. The released DC8 molecules further form solid precipitates, which exhibit brighter PL under the excitation wavelength of 473 nm (458 nm also). Similar phenomena were also observed for the DC12-CB[6]- and DC16-CB[6]-incubated cells. When DC12 or DC16 was used for imaging, they provided low imaging contrast and showed gloom (Figure S6). The toxicity of the compound decreases with the increase of the alkyl chain. Excessively long alkyl chains cause compounds to be collected, which is not conducive to cell internalization. The imaging quality can be improved when DC12-CB[6] and DC16-CB[6] were used instead of DC12 and DC16 (Figure S7).

To evidence the disassembly of DC8-CB[6] and the DC8 solid formation in cells, we employed the laser scanning confocal fluorescence imaging (Leica, STELLARIS 8)
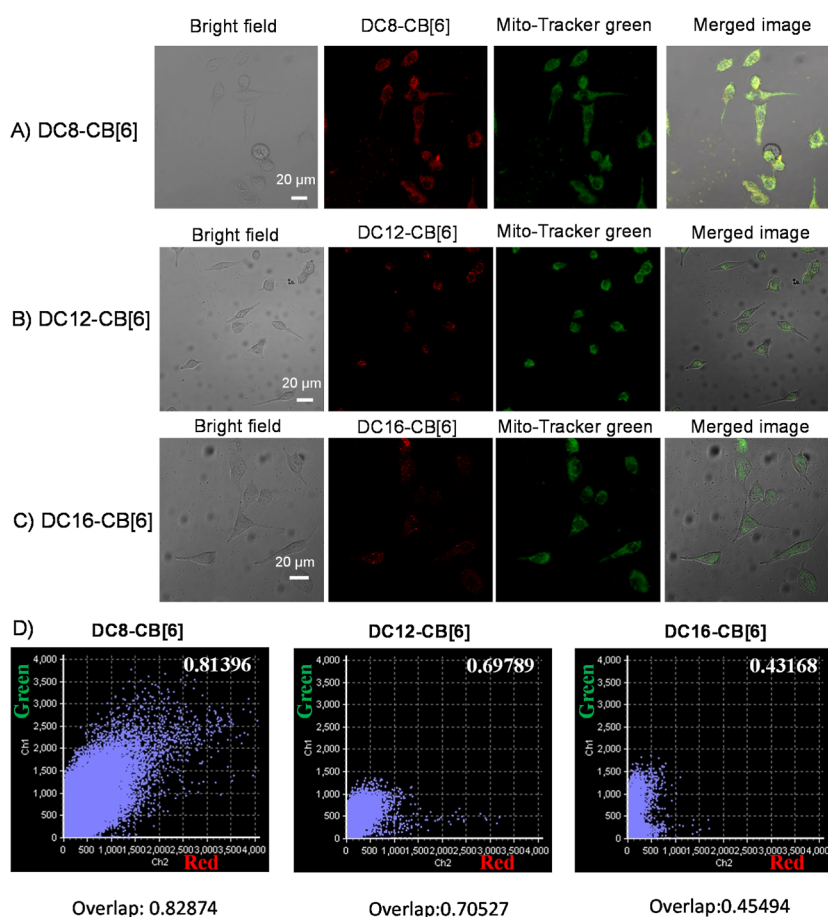
Figure 6. (A−C) Bright-field, laser scanning confocal fluorescence, merged images, and (D) colocalized scatter diagrams of MCF-7 cells after they were, respectively, incubated with DC8-CB[6], DC12-CB[6], and DC16-CB[6] (red channel, λ_{ex} = 543 nm, λ_{em} = 610 nm) and then stained with MitoTracker Green (green channel, λ_{ex} = 488 nm and λ_{em} = 500 nm), from ROIs. Pearson's correlation coefficients are calculated from (D) and marked on the scatter graphs. The overlap indices are listed on the bottom panel.

equipped with a HyD-X detector to evidence the formation of aggregation form or host−guest assembles by using the FALCON function, which allows the FLIM (Figure 4a) and quantitative analysis of lifetime of our probe. It can be observed in Figure S8 that three different lifetimes 0.348, 0.851, and 4.979 ns (χ^2 = 2.627) were fitted from the ROI of the images, which can be assigned to the DC8 solid, free DC8, and DC8-CB[6], respectively. Three lifetimes are further proven by TauSense imaging and TauSeparation function (Figure 4b). Figure 5 shows the distributions of three different lifetime components. From the left panel, we can identify the remaining DC8-CB[6] in the dish after washing, and some of them adhered to the cell membrane. The middle panel shows the mitochondria highlighted with the DC8 solid. The right panel presents the DC8 molecules, which display the longest lifetime (about 5 ns). They exhibited a distinct spatial distribution compared to the DC8 solid. Owing to their alkyl chain of DC8, individual DC8 molecules prefer to embed in the hydrophobic and phospholipid-rich regions, for example, cell membranes and nuclear membranes. These data indicate our probe DC8-CB[6], its disassembly, and DC8 solid coexisting in living cells, and three forms in a cell have different spatial distributions.

The fluorescence colocalization imaging confirmed the intracellular locations of DC8-CB[6]. We stained the cells with MitoTracker Green (mitochondrial green fluorescent probe) for DC8-CB[6] incubated with MCF-7, and the fluorescence confocal images at two channels were obtained (Figure 6A). Under the excitation light of 543 nm, orange fluorescence derived from DC8 was excited, while the excitation light of 488 nm illuminated the green fluorescence for the MitoTracker Green (mitochondria locations). These two channels show a large overlapping extent, and the Pearson correlation coefficient is calculated as 0.81396, indicating that most DC8-CB[6] have been internalized in mitochondria and showing the mitochondrion-targeting feature.[48,49]

Also, from the high-magnification images (Figure S9) and the FLIM images (Figure 4a), we can identify that the illuminated regions are typical mitochondria. The mitochondrial cristae and their morphology can be distinguished, indicating the excellent targeting feature of our probe for mitochondria.

Besides DC8-CB[6], the question of whether DC12-CB[6] and DC16-CB[6] exhibit a mitochondrion-targeting feature needs to be answered (Figure 6B,C). The allowed doses of DC12-CB[6] and DC16-CB[6] for MCF-7 cells were assessed to be 1.0 μM according to the WST-1 test (Figure S4). The Pearson correlation coefficients of DC12-CB[6] and DC16-CB[6] toward MitoTracker Green are 0.69789 and 0.43168 (Figure 6D), respectively. A decreasing trend in the mitochondrion-targeting feature (from 0.81396 to 0.43168) can be explained by the weakened dissociation ability with the

alkyl chain length. As the length of the alkyl chain increases, CB[6] tends to locate in the middle of the dipyridium compound, which causes DCn to dissociate difficultly.[44] Moreover, the potential of the series of N-alkyl pyridine bromide salt will decrease with the increase of the alkyl chain length.[30] Thus, DC8-CB[6] has a larger Pearson correlation coefficient than those of DC12-CB[6] and DC16-CB[6]. We also measured the mitochondrion-targeting feature of DC8-CB[6] in other cell lines, and the results indicate that this probe is available for enlightening the mitochondria of HepG2 cells (Figures S10 and S11).

4. CONCLUSIONS

In summary, we developed several novel supramolecular fluorescent turn-on probes composed of DCn (n = 8, 12, and 16) and CB[6]. DC8 is hydrophobic and tends to aggregate. Assembled with CB[6], the supramolecular probe shows increased dispersity and is conducive to passing through cell membranes, improving cell internalization. Interestingly, they especially exhibit mitochondrion targeting due to the positive charges of the disassembled probe. Owing to the adverse solution for DC8, they will form solid precipitates, exhibiting strong fluorescence. The supramolecular disassembly and the solid form of DC8 in cells were evidenced by FLIM analysis. Our developed supramolecular probes achieve mitochondrion-specific imaging, and they are available for the investigation of the structures and functions of mitochondria.

■ ASSOCIATED CONTENT

Ⓢ Supporting Information

The Supporting Information is available free of charge at https://pubs.acs.org/doi/10.1021/acsomega.2c03766.

> Characterizations of CB[6], fluorescence spectra of DC8 with CB[6] as different ratios, cellular toxicity of DCn and the DCn-CB[6] conjugates, fluorescence images of cells incubated with DC12 and DC16, fluorescence images of cells incubated with DC12-CB[6] and DC16-CB[6], lifetime analysis, and colocalization experiment (PDF)

■ AUTHOR INFORMATION

Corresponding Author

Shuping Xu − State Key Laboratory of Supramolecular Structure and Materials, College of Chemistry, Jilin University, Changchun 130012, P. R. China; Institute of Theoretical Chemistry, College of Chemistry and Center for Supramolecular Chemical Biology, College of Chemistry, Jilin University, Changchun 130012, P. R. China; ⊙ orcid.org/0000-0002-6216-6175; Email: xusp@jlu.edu.cn

Authors

Ning Chu − State Key Laboratory of Supramolecular Structure and Materials, College of Chemistry, Jilin University, Changchun 130012, P. R. China; Institute of Theoretical Chemistry, College of Chemistry, Jilin University, Changchun 130012, P. R. China

Lili Cong − State Key Laboratory of Supramolecular Structure and Materials, College of Chemistry, Jilin University, Changchun 130012, P. R. China

Jing Yue − State Key Laboratory of Supramolecular Structure and Materials, College of Chemistry, Jilin University, Changchun 130012, P. R. China; College of Chemical Engineering, Huanggang Normal University, Huanggang 438000, P. R. China

Weiqing Xu − State Key Laboratory of Supramolecular Structure and Materials, College of Chemistry, Jilin University, Changchun 130012, P. R. China; Institute of Theoretical Chemistry, College of Chemistry, Jilin University, Changchun 130012, P. R. China; ⊙ orcid.org/0000-0002-1947-317X

Complete contact information is available at:
https://pubs.acs.org/10.1021/acsomega.2c03766

Author Contributions

[⊥]N.C. and L.C. contributed equally to this work.

Notes

The authors declare no competing financial interest.

■ ACKNOWLEDGMENTS

■ REFERENCES

(1) Li, J.; Pu, K. Development of organic semiconducting materials for deep-tissue optical imaging, phototherapy and photoactivation. Chem. Soc. Rev. 2019, 48, 38−71.

(2) Zhang, N.; Dong, B.; Kong, X.; Song, W.; Lin, W. A two-photon endoplasmic reticulum-targeting fluorescent probe for the imaging of pH in living cells and zebrafish. Anal. Methods 2018, 10, 5702−5706.

(3) Jiao, Y.; Gong, X.; Han, H.; Gao, Y.; Lu, W.; Liu, Y.; Xian, M.; Shuang, S.; Dong, C. Facile synthesis of orange fluorescence carbon dots with excitation independent emission for pH sensing and cellular imaging. Anal. Chim. Acta 2018, 1042, 125−132.

(4) Hai, M.; Zhang, Q.; Li, Z.; Cheng, M.; Kuehne, A. J. C.; Shi, F. Visualizing polymer diffusion in hydrogel self-healing. Supramol. Mater. 2022, 1, 100009.

(5) Yang, Y.; Xia, Z.; Luo, Y.; Wu, Z.; Shi, S.; Russell, T. P. Reconfigurable structured liquids. Supramol. Mater. 2022, 1, 100013.

(6) Xiao, H.; Zhang, W.; Li, P.; Zhang, W.; Wang, X.; Tang, B. Versatile Fluorescent Probes for Imaging the Superoxide Anion in Living Cells and In Vivo. Angew. Chem., Int. Ed. 2020, 59, 4216−4230.

(7) Yang, Y.; Li, R.; Zhang, S.; Zhang, X. A fluorescent nanoprobe based on cell-penetrating peptides and quantum dots for ratiometric monitoring of pH fluctuation in lysosomes. Talanta 2021, 227, 122208.

(8) Li, N.; Cui, W.; Cong, P.; Tang, J.; Guan, Y.; Huang, C.; Liu, Y.; Yu, C.; Yang, R.; Zhang, X. Biomimetic inorganic-organic hybrid nanoparticles from magnesium-substituted amorphous calcium phosphate clusters and polyacrylic acid molecules. Bioact. Mater. 2021, 6, 2303−2314.

(9) Wu, H.; Chen, M.; Xu, Q.; Zhang, Y.; Liu, P.; Li, W.; Fan, S. Switching to a "turn-on" fluorescent probe for selective monitoring of cyanide in food samples and living systems. Chem. Commun. 2019, 55, 15137−15140.

(10) Xiong, M.; Yang, Z.; Lake, R. J.; Li, J.; Hong, S.; Fan, H.; Zhang, X. B.; Lu, Y. DNAzyme-Mediated Genetically Encoded

Sensors for Ratiometric Imaging of Metal Ions in Living Cells. *Angew. Chem., Int. Ed.* **2020**, *59*, 1891−1896.

(11) Deng, F.; Liu, L.; Qiao, Q.; Huang, C.; Miao, L.; Xu, Z. A general strategy to develop cell membrane fluorescent probes with location- and target-specific fluorogenicities: a case of a Zn(2+) probe with cellular selectivity. *Chem. Commun.* **2019**, *55*, 15045−15048.

(12) Yang, Y.; Chen, S.; Ni, X. L. Anion Recognition Triggered Nanoribbon-Like Self-Assembly: A Fluorescent Chemosensor for Nitrate in Acidic Aqueous Solution and Living Cells. *Anal. Chem.* **2015**, *87*, 7461−7466.

(13) Gu, P. Y.; Wang, Z.; Zhang, Q. Azaacenes as active elements for sensing and bio applications. *J. Mater. Chem. B* **2016**, *4*, 7060−7074.

(14) Yuan, Q.; Chen, L. L.; Zhu, X. H.; Yuan, Z. H.; Duan, Y. T.; Yang, Y. S.; Wang, B. Z.; Wang, X. M.; Zhu, H. L. An imidazo[1,5-alpha]pyridine-derivated fluorescence sensor for rapid and selective detection of sulfite. *Talanta* **2020**, *217*, 121087.

(15) Su, C.; Gelius, S. S. An improved barium-rhodizonate method for determination of sulfate ion in biological fluids. *Anal. Biochem.* **2020**, *598*, 113703.

(16) Xia, Q.; Feng, S.; Hong, J.; Feng, G. Real-time tracking lysosomal pH changes under heatstroke and redox stress with a novel near-infrared emissive probe. *Talanta* **2021**, *228*, 122184.

(17) Zhu, H.; Fan, J.; Du, J.; Peng, X. Fluorescent Probes for Sensing and Imaging within Specific Cellular Organelles. *Acc. Chem. Res.* **2016**, *49*, 2115−2126.

(18) Ni, X. L.; Chen, S.; Yang, Y.; Tao, Z. Facile Cucurbit[8]uril-Based Supramolecular Approach To Fabricate Tunable Luminescent Materials in Aqueous Solution. *J. Am. Chem. Soc.* **2016**, *138*, 6177−6183.

(19) Murphy, M. P. How mitochondria produce reactive oxygen species. *Biochem. J.* **2009**, *417*, 1−13.

(20) Galluzzi, L.; Kepp, O.; Trojel-Hansen, C.; Kroemer, G. Mitochondrial control of cellular life, stress, and death. *Circ. Res.* **2012**, *111*, 1198−1207.

(21) Li, H.; Lu, Y.; Chung, J.; Han, J.; Kim, H.; Yao, Q.; Kim, G.; Wu, X.; Long, S.; Peng, X.; Yoon, J. Activation of apoptosis by rationally constructing NIR amphiphilic AIEgens: surmounting the shackle of mitochondrial membrane potential for amplified tumor ablation. *Chem. Sci.* **2021**, *12*, 10522−10531.

(22) Pan, G. Y.; Jia, H. R.; Zhu, Y. X.; Wang, R. H.; Wu, F. G.; Chen, Z. Dual Channel Activatable Cyanine Dye for Mitochondrial Imaging and Mitochondria-Targeted Cancer Theranostics. *ACS Biomater. Sci. Eng.* **2017**, *3*, 3596−3606.

(23) Lin, F.; Bao, Y. W.; Wu, F. G. Improving the Phototherapeutic Efficiencies of Molecular and Nanoscale Materials by Targeting Mitochondria. *Molecules* **2018**, *23*, 3016.

(24) Xu, M.; Ma, X.; Wei, T.; Lu, Z. X.; Ren, B. In Situ Imaging of Live-Cell Extracellular pH during Cell Apoptosis with Surface-Enhanced Raman Spectroscopy. *Anal. Chem.* **2018**, *90*, 13922−13928.

(25) Zielonka, J.; Joseph, J.; Sikora, A.; Hardy, M.; Ouari, O.; Vasquez-Vivar, J.; Cheng, G.; Lopez, M.; Kalyanaraman, B. Mitochondria-Targeted Triphenylphosphonium-Based Compounds: Syntheses, Mechanisms of Action, and Therapeutic and Diagnostic Applications. *Chem. Rev.* **2017**, *117*, 10043−10120.

(26) Lee, M. H.; Park, N.; Yi, C.; Han, J. H.; Hong, J. H.; Kim, K. P.; Kang, D. H.; Sessler, J. L.; Kang, C.; Kim, J. S. Mitochondria-immobilized pH-sensitive off-on fluorescent probe. *J. Am. Chem. Soc.* **2014**, *136*, 14136−14142.

(27) Park, I. H.; Chanthapally, A.; Zhang, Z.; Lee, S. S.; Zaworotko, M. J.; Vittal, J. J. Metal-organic organopolymeric hybrid framework by reversible [2+2] cycloaddition reaction. *Angew. Chem., Int. Ed.* **2014**, *53*, 414−419.

(28) Stojakovic, J.; Farris, B. S.; MacGillivray, L. R. Liquid-assisted vortex grinding supports the single-step solid-state construction of a [2.2]paracyclophane. *Faraday Discuss.* **2014**, *170*, 35−40.

(29) MacGillivray, L. R.; Reid, J. L.; Ripmeester, J. A. Supra-molecular Control of Reactivity in the Solid State Using Linear Molecular Templates. *J. Am. Chem. Soc.* **2000**, *122*, 7817−7818.

(30) Samanta, S. K.; Bhattacharya, S. Aggregation induced emission switching and electrical properties of chain length dependent π-gels derived from phenylenedivinylene bis-pyridinium salts in alcohol−water mixtures. *J. Mater. Chem.* **2012**, *22*, 25277.

(31) Yang, D.; Liu, M.; Xiao, X.; Tao, Z.; Redshaw, C. Polymeric self-assembled cucurbit[n]urils: Synthesis, structures and applications. *Coord. Chem. Rev.* **2021**, *434*, 213733.

(32) Gutov, A. V.; Rusanov, E. B.; Chepeleva, L. V.; Garasevich, S. G.; Ryabitskii, A. B.; Chernega, A. N. New viologen analogs: 1,4-bis[2-(pyridin-4-yl)ethenyl]benzene quaternary salts. *Russ. J. Gen. Chem.* **2009**, *79*, 1513−1518.

(33) Chu, N.; Li, A.-S.; Xu, S.-P.; Xu, W.-Q. Studies on thermochromism of 1,4-bis[2-(4-pyridyl)ethenyl]-benzene derivatives. *Chin. J. Chem. Phys.* **2021**, *34*, 343−349.

(34) Kim, J.; Jung, I. S.; Kim, S. Y.; Lee, E.; Kang, K.; Sakamoto, S.; Yamaguchi, K.; Kim, K. New Cucurbituril Homologues: Syntheses, Isolation, Characterization, and X-ray Crystal Structures of Cucurbit-[n]uril (n) 5, 7, and 8. *J. Am. Chem. Soc.* **2000**, *122*, 540−541.

(35) Choi, S.; Lee, L.; Ko, H. K.; Kim, K. Pseudopolyrotaxanes Made to Order: Cucurbituril Threaded on Polyviologen. *Macro-molecules* **2002**, *35*, 3526−3531.

(36) Stathatos, E.; Lianos, P.; Rakotoaly, R. H.; Laschewsky, A.; Zana, R. Photophysical Behavior of a New Gemini Surfactant in Neat Solvents and in Micellar Environments. *J. Colloid Interface Sci.* **2000**, *227*, 476−481.

(37) Lee, J. W.; Samal, S.; Selvapalam, N.; Kim, H.; Kim, K. Cucurbituril Homologues and Derivatives: New Opportunities in Supramolecular Chemistry. *Acc. Chem. Res.* **2003**, *36*, 621−630.

(38) Liu, M.; Zhou, Y.; Chen, L.; Bian, B.; Xiao, X.; Tao, Z. Cucurbit[n]uril-calix[n]arene-based supramolecular frameworks as-sembled using the outer surface interactions of cucurbit[n]urils. *Chin. Chem. Lett.* **2021**, *32*, 375−379.

(39) Bai, D.; Gao, Z.; Tao, Z.; Xiao, X.; Prior, T. J.; Wei, G.; Liu, Q.; Redshaw, C. A study of the interaction between inverted cucurbit[6]-uril and symmetric viologens. *New J. Chem.* **2018**, *42*, 11085−11092.

(40) Naik, V. G.; Kumar, V.; Bhasikuttan, A. C.; Kadu, K.; Ramanan, S. R.; Bhosle, A. A.; Banerjee, M.; Chatterjee, A. Solid-Supported Amplification of Aggregation Emission: A Tetraphenylethylene−Cucurbit[6]uril@Hydroxyapatite-Based Supramolecular Sensing As-sembly for the Detection of Spermine and Spermidine in Human Urine and Blood. *ACS Appl. Bio Mater.* **2021**, *4*, 1813−1822.

(41) Shan, P. H.; Tu, S. C.; Lin, R. L.; Tao, Z.; Liu, J. X.; Xiao, X. Supramolecular complexes of α,α′,δ,δ′-tetramethyl-cucurbit[6]uril binding with enantiomeric amino acids. *CrystEngComm* **2017**, *19*, 2168−2171.

(42) Xiao, X.; Gao, Z. Z.; Shan, C. L.; Tao, Z.; Zhu, Q. J.; Xue, S. F.; Liu, J. X. Encapsulation of haloalkane 1-(3-chlorophenyl)-4-(3-chloropropyl)-piperazinium in symmetrical alpha,alpha',delta,delta'-tetramethyl-cucurbit[6]uril. *Phys. Chem. Chem. Phys.* **2015**, *17*, 8618−8621.

(43) El-Barghouthi, M. I.; Abdel-Halim, H. M.; Haj-Ibrahim, F. J.; Assaf, K. I. Molecular dynamics simulation study of the structural features and inclusion capacities of cucurbit[6]uril derivatives in aqueous solutions. *Supramol. Chem.* **2014**, *27*, 80−89.

(44) He, S.; Zhou, C.; Zhang, H.; Zhou, X. Binding modes of cucurbit[6]uril and cucurbit[7]uril with a series of bis-pyridinium compounds. *J. Inclusion Phenom. Macrocyclic Chem.* **2012**, *76*, 333−344.

(45) Yu, D. H.; Ni, X. L.; Tian, Z. C.; Zhang, Y. Q.; Xue, S. F.; Tao, Z.; Zhu, Q. J. Host−guest inclusion complexes of four partial alkyl-substituted cucurbit[6]urils with some probe guests. *J. Mol. Struct.* **2008**, *891*, 247−253.

(46) Klöck, C.; Dsouza, R. N.; Nau, W. M. Cucurbituril-Mediated Supramolecular Acid Catalysis. *Org. Lett.* **2009**, *11*, 2595−2598.

(47) Zhao, N.; Liu, L.; Biedermann, F.; Scherman, O. A. Binding studies on CB[6] with a series of 1-alkyl-3-methylimidazolium ionic liquids in an aqueous system. *Chem.—Asian J.* **2010**, *5*, 530−537.

(48) Gao, G.; Jiang, Y. W.; Yang, J.; Wu, F. G. Mitochondria-targetable carbon quantum dots for differentiating cancerous cells from normal cells. *Nanoscale* **2017**, *9*, 18368−18378.

(49) Hua, X. W.; Bao, Y. W.; Chen, Z.; Wu, F. G. Carbon quantum dots with intrinsic mitochondrial targeting ability for mitochondria-based theranostics. *Nanoscale* **2017**, *9*, 10948−10960.